Towards the measurement of the $t\bar{t}$ cross section in the tau dilepton channel in pp collisions

Marcelo Guerra Jordão
Instituto Superior Técnico - Mestrado em Engenharia Física Tecnológica
(Dated: November 2009)

The LHC will be a top quark factory, requiring the full exploitation of all available channels. The tau leptons (τ) will show up in final state of several physics processes at LHC, and particularly, the presence of taus in top decays will allow to set limits on predictions beyond Standard Model. Therefore, the development of an efficient and accurate reconstruction and identification of hadronicaly decaying taus at CMS detector is one of the most challenging and interesting tasks at the hadron collider. The work presented in this thesis aims towards the measurement of the $t\bar{t}$ cross section with channels involving taus, taking special attention on the optimisation of the tau reconstruction algorithm, with the early data taking phase of CMS detector, as well as the exploitation of data driven methods to estimate the background contamination in taus.

1. INTRODUCTION

The observation of the top quark is the latest in a long series of triumphs for the Standard Model of particles and fields that has culminated, in 1995, with the discovery of this particle in proton-antiproton ($p\bar{p}$) collisions at the Tevatron.

The top quark is the heaviest fermion particle predicted by the Standard Model, and was the last fundamental particle found. The search for the top quark was an arduous process due to the high mass difference between his least-heavy partner, the bottom quark, ($M_{top} \approx 40 \cdot M_{bottom}$ [1]). This mass difference is one of the deepest physics mysteries, remaining an unanswered question in particle physics.

The potential for measure the $t\bar{t}$ cross section at the CERN LHC (Large Hadron Collider) with the CMS (Compact Muon Solenoid) detector is exploited, using channel as signature, the taus in the top pair decay chain.

1.1. Top quark at LHC

Almost 15 years have passed after the discovery of the top quark at the CDF [2] and DØ [3] experiments at the Tevatron. As a major goal, the Large Hadron Collider (LHC), located at CERN in Geneva-Switzerland, looks forward for the rediscovery of the top quark and characterize the proprieties of this particle, that is the heaviest known fermion predicted by the Standard Model.

Most of the top quarks at the LHC will be produced as $t\bar{t}$ pairs at a very high rate. These $t\bar{t}$ processes generally involve high transverse momentum observables, as a product decay from top quark, before hadronization. The detectors will exploit all the decay channels from this process, using the available observables to measure the production cross section as well as mass and spin proprieties of the top quark.

Most of the top quarks at the LHC will be produced as $t\bar{t}$ pairs. At the centre-of-mass energy $\sqrt{s} = 14$ TeV, the $t\bar{t}$ production cross section is estimated to be 830 pb [4] for NLO calculations. The $t\bar{t}$ pairs can be produced by quark-anti-quark annihilation ($\approx 10\%$) mechanisms (Fig. 1(a)), but the dominant production at LHC will be by gluon-gluon fusion ($\approx 10\%$) (Fig. 1(b)).

While the LHC was originally conceived to operate at an centre-of-mass of $\sqrt{s} = 14$ TeV, this goal wont be possible for the startup period. The machine will need to be tested and tuned up, before it can run at full energy and luminosity operation, thus, during the first period of data taking, the LHC is expected to run at a lower centre-of-mass energy $\sqrt{s} = 7 - 10$ TeV. The results are normalized to the first 200 pb^{-1} of data ($\approx$ one year of LHC operation at $\sqrt{s} = 10$ TeV), and the cross section is estimated to be $\sigma_{t\bar{t}} = 414^{+41}_{-42}$ pb [5] at NLO.

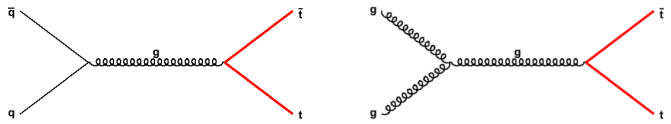

(a) $t\bar{t}$ pair produced through quark-anti-quark annihilation.

(b) $t\bar{t}$ pair produced through gluon-gluon fusion.

Figure 1: Production of top quark pair through gluon fusion (1(b)) and quark/anti-quark annihilation (1(a)) mechanisms.

Within the Standard Model the top quark decays almost exclusively to a W boson and a b quark. The decays of $t\bar{t}$ system are then classified according to the decays of W^+W^- system, as dileptonic, semi-leptonic or fully hadronic. The W boson can decay into leptons, $(e^-\overline{\nu}_e), (\mu^-\overline{\nu}_\mu)$ and $(\tau^-\overline{\nu}_\tau)$, or into quark systems, $(u\bar{d})$ and $(c\bar{s})$, where the charge conjugate is implicit. As the top is a heavy quark ($M_{top} \approx 2.15 \cdot M_W$ [1]), it decays promptly without hadronizing.

1.2. Top quark signatures

Due to their mass, the top quarks decay with a very short lifetime, not hadronizing in the calorimeters. Therefore, to understand the experimental signature for a top event, it is necessary to understand the decay modes of the $t\bar{t}$ system.

At LHC energies, the $t\bar{t}$ signature ($pp \rightarrow t\bar{t}$) will be the most important mechanism for producing top quarks (in pairs), and overlaps the single top production ($pp \rightarrow W \rightarrow t\bar{b}$).

Accordingly with the Standard Model, the top quark decays as $t \rightarrow Wb$. The W will subsequently decay into fermion pairs, either $W \rightarrow \ell\nu$ or $W \rightarrow q\bar{q}$, where ℓ denotes a lepton (e, μ, or τ), and $q\bar{q}$ denotes a light quark pair, either $u\bar{d}$ or $c\bar{s}$. As the decay modes of the W boson pair determine the observed event signatures, the "standard dilepton" decay channel denotes the case where both W bosons decay into leptons, i.e. to electrons or muons plus corresponding neutrinos. The decay chain is:

$$t\bar{t} \rightarrow WW\ (b\bar{b}) \rightarrow (\ell\nu_\ell)\ (\ell\nu_\ell)\ (b\bar{b}) \text{ where } (\ell = e, \mu). \quad (1)$$

1.3. Tau dilepton: $t\bar{t}$ with taus

In the "tau dilepton" channel, only a single W decays into $e\nu_e$ or $\mu\nu_\mu$, while the other decays into the third generation leptons $\tau\nu_\tau$. Consequently the total decay chain is:

Table I: Decay modes for a $t\bar{t}$ pair and their lowest order branching ratios assuming Standard Model, performing a total of 81 modes.

Channel name	Decay mode	Branching ratio
Hadronic	$t\bar{t} \to WW\ (b\bar{b}) \to (q\bar{q})\ (q\bar{q})\ (b\bar{b})$	36/81
Semi-Leptonic	$t\bar{t} \to WW\ (b\bar{b}) \to (q\bar{q})\ (e\nu)\ (b\bar{b})$	12/81
	$t\bar{t} \to WW\ (b\bar{b}) \to (q\bar{q})\ (\mu\nu)\ (b\bar{b})$	12/81
	$t\bar{t} \to WW\ (b\bar{b}) \to (q\bar{q})\ (\tau\nu)\ (b\bar{b})$	12/81
Standard Dieptonic	$t\bar{t} \to WW\ (b\bar{b}) \to (e\nu)\ (e\nu)\ (b\bar{b})$	1/81
	$t\bar{t} \to WW\ (b\bar{b}) \to (\mu\nu)\ (\mu\nu)\ (b\bar{b})$	1/81
	$t\bar{t} \to WW\ (b\bar{b}) \to (\tau\nu)\ (\tau\nu)\ (b\bar{b})$	1/81
	$t\bar{t} \to WW\ (b\bar{b}) \to (e\nu)\ (\mu\nu)\ (b\bar{b})$	2/81
Dileptonic w/ Taus	$t\bar{t} \to WW\ (b\bar{b}) \to (e\nu)\ (\tau\nu)\ (b\bar{b})$	2/81
	$t\bar{t} \to WW\ (b\bar{b}) \to (\mu\nu)\ (\tau\nu)\ (b\bar{b})$	2/81

$$t\bar{t} \to \mathrm{WW}\ (b\bar{b}) \to (\ell\nu_\ell)\ (\tau\nu_\tau)\ (b\bar{b}) \text{ where } (\ell = e, \mu). \quad (2)$$

The total branching ratio of the $t\bar{t}$ system to "tau dilepton" channel is:

$$\begin{aligned} \mathrm{BR}_{t\bar{t}\to(\ell\nu_\ell)(\tau\nu_\tau)b\bar{b}} &= 2 \cdot \mathrm{BR}_{W\to\ell\nu_\ell} \cdot \mathrm{BR}_{W\to\tau\nu_\tau} \cdot \mathrm{BR}_{\tau\to\mathrm{had}} \\ &+ 2 \cdot \mathrm{BR}^2_{W\to\tau\nu_\tau} \cdot \mathrm{BR}_{\tau\to\mathrm{had}} \cdot \mathrm{BR}_{\tau\to\ell\nu_\ell} \end{aligned} \quad (3)$$

The expected "tau dilepton" ($e\tau$, $\mu\tau$) rate is approximately 5% (4/81) of all $t\bar{t}$ decays, which is equivalent to the "standard dilepton" (ee, $\mu\mu$, $e\mu$). Performing a test of lepton universality in top quark decay final states and, in particular, the measurement of $\mathrm{BR}_{t\bar{t}\to(\ell\nu_\ell)(\tau\nu_\tau)b\bar{b}}/\mathrm{BR}_{t\bar{t}\to(\ell\nu_\ell)(\ell\nu_\ell)b\bar{b}}$ may help setting limits on new non-SM physics processes.

The "tau dilepton" channel is of particular interest because the existence of a charged Higgs with $m_H < m_{top}$ could give rise to anomalous tau lepton production, which could be directly observable in this decay channel. At the Tevatron (CDF and DØ experiments in Fermilab) only a few events have been observed in the top dilepton channel with tau leptons in the final state [6, 7]. Understanding tau production is therefore important for several reasons: **a)** to check universality of lepton couplings, **b)** to increase acceptance for $t\bar{t}$events, and **c)** to search for new physics processes.

2. EXPERIMENTAL APPARATUS

2.1. The Large Hadron Collider

The Large Hadron Collider (LHC), at the European Centre for Nuclear Research (CERN) Laboratory, located near Geneva, Switzerland is the world's largest complex for particle physics research. It is a unique tool for fundamental physics discoveries, with the highest energy particle acceleration in the world for many years after its completion. The LHC was projected and constructed in the existing 27-Km LEP tunnel and is designed for collisions of proton and ion beams of 7 TeV and 2.75 TeV respectively, with a conceived luminosity of 10^{34} $\mathrm{cm^{-2}s^{-1}}$(10 $\mathrm{nb^{-1}}$) for protons, and 10^{27} $\mathrm{cm^{-2}s^{-1}}$(1 $\mathrm{mb^{-1}}$) for heavy ions.

The LHC will provide two proton beams, circulating in opposite directions, at energies up to 7 TeV each (centre-of-mass $\sqrt{s} = 7 - 14$ TeV. It is expected that the data produced at the LHC will elucidate the electroweak symmetry breaking mechanism (EWSM) and provide evidence of physics beyond the Standard Model. The LHC will be afterwards a Z factory, a W factory, a bottom-quark factory and a top-quark factory. Also a Higgs boson or SUSY sparticle factory, if these particles have TeV scale masses.

The machine is currently under final adjustments for the start of proton proton collisions. After a long period of tuning and delays, the beginning of operation is expected to happen, at lower energy proton beams (3.5 TeV each), in November 2009.

2.2. The CMS Detector

The Compact Muon Solenoid (CMS) detector is a general purpose apparatus designed to operate at the LHC. The CMS is installed about 100 meters underground in the French village of Cessy between Lake Lèman and the Jura mountains. The detector requirements for CMS to meet the goals of the LHC physics program can be summarized as follows:

- Good muon identification with a momentum resolution over a wide range of momenta and angles. Dimuon mass resolution $\approx$ 1% at 100GeV/c with the capability to determine unambiguously the charge of muons with p < 1TeV;
- Good electromagnetic energy resolution with a high granularity electromagnetic calorimeter, with a diphoton/dielectron mass resolution $\approx$ 1% at 100GeV, in a wide geometric coverage. Efficient photon and lepton isolation, with π^0 identification;
- High resolution on the missing transverse energy ($\not{E}_T$) of events and high dijet-mass definition, requiring hadron calorimeters with large hermetic geometric coverage and with fine lateral segmentation;
- Capability on offline tagging of τ-jets and b-jets, requiring pixel detectors close to the interaction region. Good charged-particle momentum and energy resolution and efficiency in the inner tracker;

The design of CMS meets these requirements, and the analysis presented in this thesis requires all those detector requirements. This analysis involves lepton and jet identification and also high level tau tagging and b tagging. The missing transverse energy ($\not{E}_T$) is also presented in $t\bar{t}$ decays due to neutrinos.

This detector meets the general requirements to fulfill the needs of high energy analysis in hadronic collisions and the

main distinguish features of CMS are a high-field solenoid, a full-silicon-based inner tracking system, and a homogeneous scintillating-crystals-based electromagnetic calorimeter.

An important aspect driving the detector design and layout is the choice of the magnetic field configuration for the measurement of the momentum of muons. Large bending power is needed to measure the momentum of high energy charged particles. This forced a choice of superconducting technology for the magnets.

The layout of CMS is shown in Fig. 2. At the hearth of CMS exist a 13 m long and 6 m inner diameter, 4 Tesla superconducting solenoid, providing a large bending power (12Tm) before the muon bending angle is measured by the muon system. The return field is large enough to saturate 1.5 m of iron, allowing 4 muon stations to be integrated to ensure robustness and full geometric coverage. Each muon station consists of several layers of aluminium drift tubes (DTs) in the barrel region an cathode strip chambers (CSCs) in the endcap regions, complemented by resistive plate chambers (RPCs). The overall dimensions of the CMS detector are a length of 21.6 m, a diameter of 14.6 m and a total weight of 12500 tons.

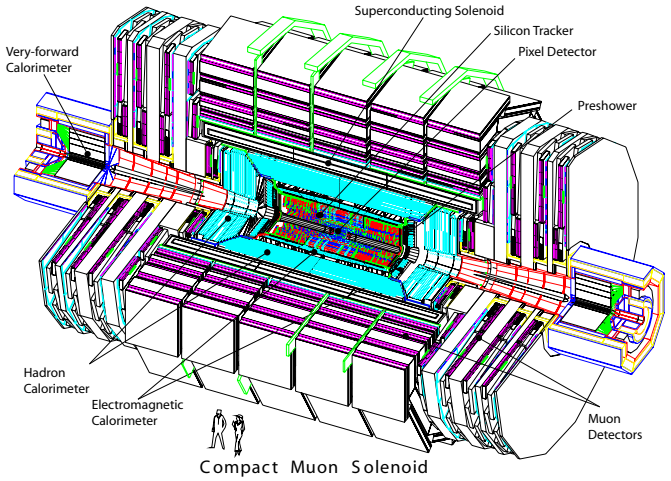

Figure 2: CMS detector layout, with all subdetector components.

The bore of the magnet coil is also large enough to accommodate the inner tracker and the calorimetry inside. The tracking volume is given by a cylinder of length 5.8 m and diameter 2.6m. In order to deal with high track multiplicities, CMS employs 10 layers of silicon microstrip detectors, which provide the required granularity and precision. In addition, 3 layers of silicon pixel detectors are placed close to the interaction region to improve the measurement of the impact parameter of charged-particle tracks, as well as the position of secondary vertices.

The EM calorimeter (ECAL) uses lead tungstate ($PbWO_4$) crystals with coverage in pseudo-rapidity up to $|\eta| < 3.0$. The scintillation light is detected by silicon avalanche photodiodes (APDs) in the barrel region and vacuum phototriodes (VPTs) in the endcap region. A pre-shower system is installed in front of the endcap ECAL for π^0 rejection.

The ECAL is surrounded by a brass/scintillator sampling hadron calorimeter (HCAL) with coverage up to $|\eta| < 3.0$. The scintillation light is converted by wavelength-shifting (WLS) fibres embedded in the scintillator tiles and channeled to photodetectors via clear fibres.

This light is detected by novel photodetectors (hybrid photodiodes, or HPDs) that can provide gain and operate in high axial magnetic fields. This central calorimetery is complemented by a "tail-catcher" in the barrel region, ensuring that hadronic showers are sampled with nearly 11 hadronic interaction lengths. Coverage up to a pseudo-rapidity of 5.0 is provided by an iron/quartz-fibre calorimeter. The Cherenkov light emitted in the quartz fibres is detected by photomultipliers.

The forward calorimeters ensure full geometric coverage for the measurement of the transverse energy in the event.

3. OBJECT RECONSTRUCTION

The reconstruction of physics objects, such as leptons (e, μ, τ), jets, missing transverse energy ($\not{E}_T$), and b-tagging, are performed with common tools and software standard for CMS physics. The object reconstruction tools are implemented by CMS Physics Object Groups (`POGs`), with common standard layers, that can be used for various physics analysis purposes. Several versions of CMS Software have been used, due to a constant evolution and optimization of these tools during the content development time of this thesis. But the basis of the analysis is CMS Software Version 2.2.10 (`CMSSW_2_2_10`) [8] with standardized Physics Analysis Toolkit (`PAT`) [9] objects were used to performed this study.

3.1. Lepton reconstruction

Electrons are reconstructed as `PixelMatchGsfElectrons` with cut-based electron-ID [10, 11] as defined by the e-gamma `POG`. The **eidTight** category has a low fake rate ($\sim 10^{-4}$), when compared with other electron-ID categories (approximately 10 times smaller than the **eidRobustHighEnergy**) and is preferred for electron selection having an efficiency above 80%, for $p_T \geq 20$ GeV/c (Fig. 3).

The efficiency of electron reconstruction for different categories as a function of the pseudo-rapidity is approximately constant and above 80% in the Barrel ($|\eta| < 1.6$), while it decreases in the Endcaps ($|\eta| > 1.6$).

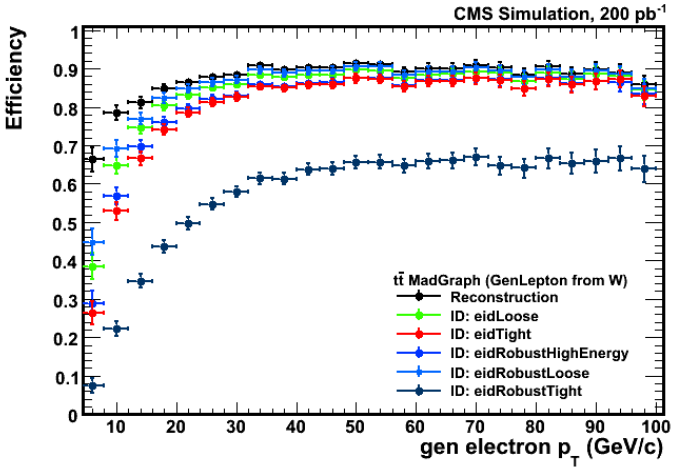

Figure 3: Efficiency as function of generated electron p_T for different electron reconstruction categories.

Muons are selected from the `globalMuons` collection, built by the match of "hits" in the muon chambers with trajectories in the tracker detector. A Kalman filter technique [12] combines data from `standaloneMuons` and `trackerMuons` collections. The hits from muon sub-detector are fitted with data coming from tracker and this extrapolation is the `globalMuons` collection.

Results show that muon efficiencies are above 90% for $p_T \geq$ 20 GeV/c (Fig. 4) without requiring any quality cuts.

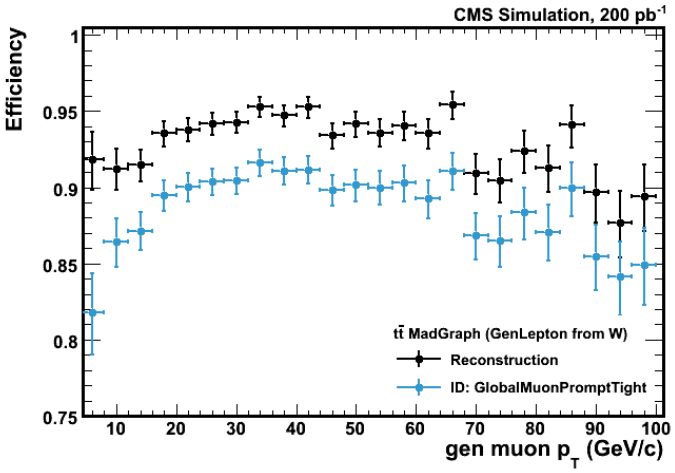

Figure 4: Efficiency as function of generated muon p_T for different electron reconstruction categories.

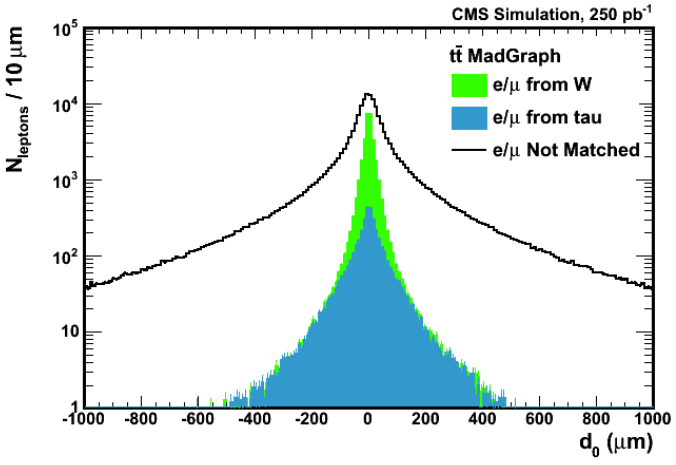

Figure 5: Impact parameter (d_0) of lepton candidates (e or μ) in $t\bar{t}$ events. A cut at $|d_0| < 400$ μm has an efficiency of 99% for matched leptons matched, rejecting approximately 10% of the background leptons.

After requiring the **globalMuonPromptTight** category recommended by the muon POG, (at least 10 hits in muon subdetector and a χ^2/ndof < 10), the efficiency lowers by 5%, while the fake rate is reduced by a factor of ~ 10. The efficiency of electron/muon identification and reconstruction will be estimated with early data using the "tag and probe" method with $Z \rightarrow (e, e)/(\mu\mu)$ events [12].

Isolation cuts are applied to electron and muon candidates, in order to distinguish leptons from W decays, from leptons in jets, which originate from semi-leptonic b/c-hadron decays. Tracker isolation is defined as the fraction of transverse momentum carried by the track associated to the lepton candidate with respect to the total transverse momentum found inside a cone of size $\Delta R = 0.3$ around the lepton direction, where $\Delta R = \sqrt{\eta^2 + \phi^2}$ excluding the lepton track. It is satisfied when relative value is larger than 0.9 for electrons and muons ($iso_{track} : \frac{p_T(lepton)}{p_T(lepton)+\sum p_T^{track}} > 0.9$), yielding an efficiency above 90%.

Calorimeter isolation variable is defined as the sum of energies of all calorimeter towers around the lepton direction, excluding the lepton energy deposited in the calorimeter, and it is required to be larger than 0.8(0.9) for electrons(muons) ($iso_{calo} : \frac{p_T(lepton)}{p_T(lepton)+\sum E_T^{calo}} > 0.8(0.9)$).

The tau dilepton channel is characterized by the presence in the final state of at least one high p_T lepton (electron or muon). Therefore, a tight selection on kinematic parameters from leptons is required in order to remove low p_T objects that may fake the signal selection.

The track associated to each lepton candidate is required to have an impact parameter compatible with prompt production: $|d_0| < 400$ μm (measured with respect to the primary vertex of the hard interaction). The distribution of the lepton track impact parameter with respect to the primary vertex is shown in Fig. 5. The cut at $|d_0| < 400$ μm removes significant contamination of non-prompt leptons.

3.2. Jet reconstruction

As the top quark decays, through weak process ($t \rightarrow Wb$), two jets from b-quark hadronization appear in the event signature. Jets are reconstructed from the calorimetric energy deposits using the Seedless Infrared Cone (SIS) [13] algorithm with a radius of R = 0.5 where $R = \sqrt{\eta^2 + \phi^2}$ is the jet aperture. Track are associated to the calorimeter jet if they are in a cone of radius R = 0.5 surrounding the jet axis. Only calorimeter cells with a minimum energy deposit of 1 GeV are used as jet seeds.

The energy of jets in the event is corrected for variations with pseudo-rapidity $|\eta|$ and for absolute transverse momentum p_T [14]. After applying these corrections, jets are selected by requiring a $p_T^{(corrected)} \geq 30$GeV/c and $|\eta| < 2.4$. To remove isolated lepton fakes, jet candidates are required to be separated, in $\eta - \phi$ space, by a $\Delta R(\text{jet} - \text{lepton}) \geq 0.3$ and a electromagnetic fraction EMF < 0.98, taking into account the narrow jets, where energy is mostly concentrated around the isolated lepton thrust.

Two jets in the $t\bar{t}$ events are from b-quark jets. Requiring one or more jets to be b-tagged improves the S/B ratio, although the signal efficiency is lower. A b-tagging algorithm [15] based on the identification of tracks with large impact parameter is used to identify the jet flavor, and the method efficiency to derive its efficiency from $t\bar{t}$ dilepton eμ channel is presented in [16].

3.3. Missing transverse energy

The missing transverse energy $\not{E}_T$ in the event, mainly due to neutrinos, is reconstructed using calorimeter towers and muon information, from the transverse vectorial sum of calorimetric energy deposits. The $\not{E}_T$ is corrected based on jet corrections with $p_T > 20$ GeV/c and $|\eta| < 2.5$, taking into account the momenta of reconstructed muons with $p_T > 20$ GeV/c and $|\eta| < 2.5$ that are not detected by the calorimeters [17].

Both H_T and $\not{E}_T$ variables have been studied in order to improve the rejection of the W/Z+jets background. The total transverse energy H_T is defined as the scaler sum of all transverse energies in the event, as show in Eq. 4.

$$H_T = p_T^{e,\mu} + p_T^{\tau} + \not{E}_T + \Sigma p_T^{jets} \quad (4)$$

All isolated electrons/muons ($p_T > 20$ GeV/c, $|\eta| < 2.4$),

all taus ($p_T^{leadTk} < 20$ GeV/c, $|\eta| < 2.4$ including electron/muon rejection cuts), all jets ($E_T > 30$ GeV/c, $|\eta| < 2.4$), and $\not{E}_T$ are included in the calculation of H_T. The $\not{E}_T$ variable is preferred over H_T to reject the W/Z+jets background, and a cut $\not{E}_T > 40$ GeV is chosen to be consistent with other top analyses.

4. TAU IDENTIFICATION

Tau identification is challenging at an hadron collider. Jets originated from quarks and gluons may be misidentified as taus. Using the `CaloTau` algorithm[18], tau candidates are reconstructed using basic tracking and calorimeter information. For each jet reconstructed in the event, the `CaloTau` algorithm seeks a nearby tracks within a matching cone ($\Delta R < 0.1$ from the jet's axis). The track with the highest p_T is chosen to be the leading track. All tracks with $p_T > 1$ GeV/c within a "signal" cone of $R = 0.07$ around the leading track are considered. The object is identified as a tau if there are no additional tracks with $p_T > 1$ GeV/c in the isolation cone ($0.07 < \Delta R < 0.5$).

Tau candidates with transverse momentum of the leading track $p_T^{leadTk} > 20$ GeV/c and in fiducial area of $|\eta| < 2.4$ are selected. Additional calorimeter information of the energy cluster matched to the reconstructed track(s) is used to further reject contamination of electrons and muons of the tau-tagged objects. In order to optimize the electron and muon (as well as jet) veto cuts, matching to generator level objects in the $t\bar{t}$ MadGraph sample was used.

For each jet reconstructed in the event, this `CaloTau` algorithm seeks for a nearby tracks, within a matching cone. The track from this collection, with higher pT, is chosen to be the leading track. Tracks are considered "seeds" if they have a transverse momentum above the threshold, and if a jet is found within a cone of $\Delta R = 0.1$. All tracks with $p_T > 1$ GeV/c within a cone of delta $R = 0.7$ are added to the seed. To tight this selection for lower QCD jets fake rates, this object is identified as a tau, if there are no additional tracks with $p_T > 1$ GeV/c in the isolation cone of $\Delta R = 0.1$.

4.1. Tracking and calorimeter isolation

Isolation is a powerful discriminant against jets in QCD processes. Tau leptons have small track multiplicity (1- or 3-prongs), generally producing narrow energy deposits in the electromagnetic and hadronic calorimeters, whereas QCD jets are wider and with higher track multiplicity. In the optimization of hadronic tau reconstruction/identification algorithm several studies have been performed in order to obtain the best isolation value, with a good compromise between large background rejection and reasonable signal efficiency.

The sum of transverse momentum ($\Sigma p_T^{iso=0.5} = 0$) from tracks in the isolation cone (i.e. $0.07 < \Delta R < 0.5$), equivalent to requiring no jets inside the annulus, is an excellent jet discriminator.

Additional rejection of QCD jets can be achieved by requiring the jet to be isolated in the electromagnetic calorimeter (ECAL isolation), without significantly reducing the tau efficiency. The sum of the electromagnetic energy ($\Sigma E_T^{iso=0.5}$) inside the ECAL annulus region is smaller for hadronic taus than for jets.

4.2. Lepton vetoes

The tau reconstruction algorithm sometimes erroneously selects electron or muons, instead of hadronically decaying tau leptons. The use of the calorimeter and tracker information can help in discriminating electron, muons, and taus.

Electrons produce localized energy deposits in electromagnetic calorimeters (E_{ECAL}^{jet}), matched with a track in the silicon detector, and very small (or none) energy deposit in the hadronic calorimeter (E_{HCAL}^{jet}). These electrons, can be reconstructed as hadronically decaying tau leptons due to the electromagnetic behavior, electrons will produce electromagnetic cascades in ECAL. The energy clusters from reconstructed jets have electromagnetic fraction EMF ≈ 1, and small energy deposits in the hadronic calorimeter $E_{HCAL}^{jet} \approx 0$.

The electromagnetic fraction (Eq. 5) for electrons is expected to be approximately one.

$$\text{EMF} : \frac{E_{ECAL}^{jet}}{E_{ECAL}^{jet} + E_{HCAL}^{jet}} \tag{5}$$

In Fig. 6 is presented the electromagnetic fraction EMF for reconstructed taus, matched with generated electrons and hadronic taus in a $t\bar{t}$ sample. Hadronic taus have flat distribution, while electrons peaks at EMF ≈ 1, as expected.

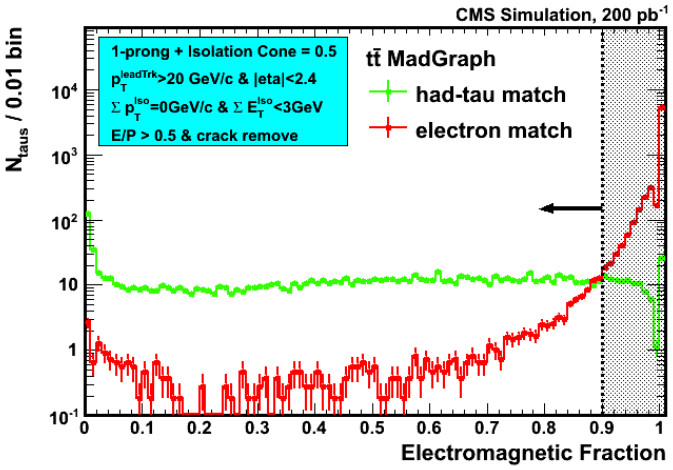

Figure 6: Calorimeter information associated to the tau energy cluster. Electromagnetic fraction (EMF).

Energy clusters with EMF ≥ 0.9 are vetoed as electrons. This cut remove $\approx 98.5\%$ of the electron contamination in tau tagged objects.

Muons can also contaminate the tau-tagged sample. Tracks in the silicon detector associated with small amounts of energy deposits on electromagnetic and hadronic calorimeters. The total cluster energy (E), defined as the sum of the energies in the electromagnetic (ECAL) and hadronic (HCAL) calorimeters, divided by the track total momentum (p) is shown in Fig. 7 (left).

$$\text{E/P} : \frac{E^{jet}}{p^{leadTk}} \tag{6}$$

The cut E/P > 0.5 has high efficiency for hadronic taus ($\approx 99.7\%$), while being a powerful discriminant against muons.

Fig. 7 (right) shows the 2-dimensional scatter plot of the EMF versus E/P distributions for electrons, muons and taus separately. Electrons are mostly concentrated in high values

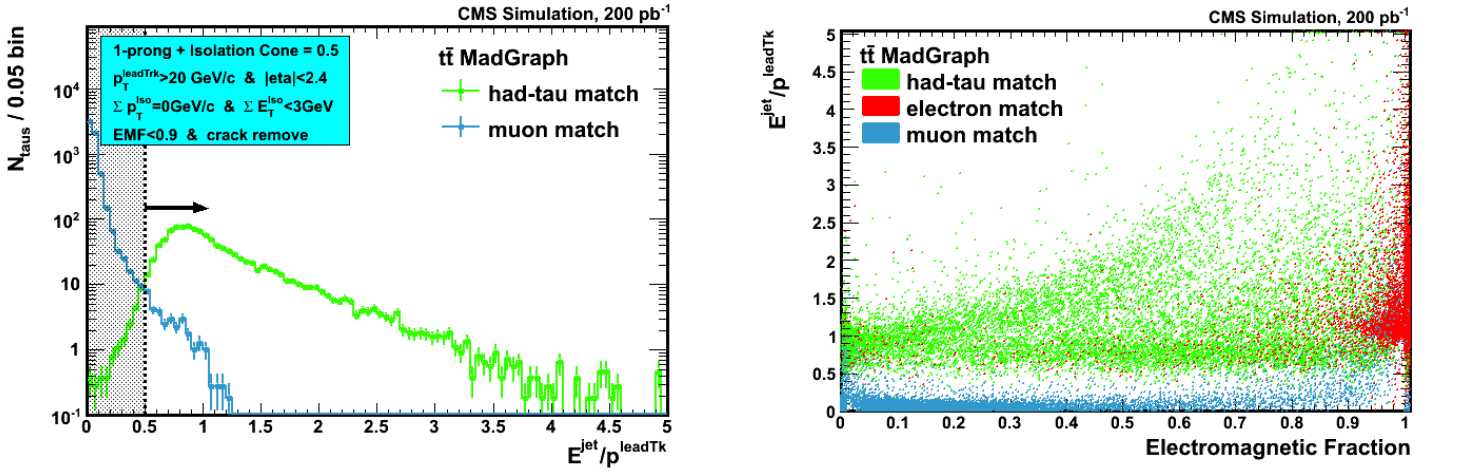

Figure 7: Calorimeter information associated to the tau energy cluster (E/P) (left) and EMF versus E/P distributions for taus electrons, muons and taus (right).

of electromagnetic fraction (EMF $\approx$ 1) and in (E/P $\approx$ 1) while muons appear in the low values of E/P. Taus are spread all over the E/P vs. EMF plane, but mostly outside the considered veto regions.

5. EVENT SELECTION

The $t\bar{t}$ dilepton events are characterized in the final state, by the presence of two leptons from prompt W decays. In particular the tau dilepton has, one light lepton, either an electron or muon, and also a third generation tau lepton, that originate a jet from their hadronic decays.

Additionally, two jets from b-quark hadronization are produced along with the leptons. Due to the existence of neutrinos in the $t\bar{t}$ dilepton decay chain, rising from leptonic W decays and from jet hadronizations, the event is marked by the presence of missing transverse energy ($\not\!\!E_T$).

Events are selected by requiring at least one high-p_T ($p_T >$ 20 GeV/c), isolated lepton in fiducial area of $|\eta| < 2.4$. To reject Minimum Bias and QCD processes contamination, it is required that $t\bar{t}$ tau dilepton event signature have two high-p_T jets with ($p_T >$ 30GeV/c and $|\eta| < 2.4$), large missing transverse energy ($\not\!\!E_T >$ 40GeV), and one tau lepton. All objects are separated in $\eta - \phi$ space by $\Delta R > 0.3$.

The two high-p_T isolated leptons in $t\bar{t}$ dilepton events come from two W bosons and are required to be oppositely charged.

The charge of the tau object is defined as the charge of the leading track, since the charge of a jet cannot be defined with a calorimeter variables that compose the jet.

5.1. Event yields

The selection up to missing transverse energy ($\not\!\!E_T >$ 40 GeV) cut is denominated by Trigger plus W+jets-like selection and is summarized in Tab. II includes:

- Trigger: HLT_Mu9 **OR** HLT_Ele15_LW_L1R;
- $N_{lep} \geq 1$: at least one isolated lepton (e/μ) w/ $p_T >$ 20 GeV/c, $|\eta| < 2.4$, $iso_{track} > 0.9$, $iso_{calo} > 0.8(0.9)$;
- $N_{jet} \geq 2$: at least two jets with $p_T > 30$ GeV/c, $|\eta| <$ 2.4;
- $\not\!\!E_T > 40$ GeV.

Only significant backgrounds are shown, W+jets, Z($\ell\ell$)+jets, Single Top, QCD. The Z($\tau\tau$)+jets is an important and irreducible source of background, when one of the taus decay leptonically and the other decays hadronically.

After the missing transverse energy cut ($\not\!\!E_T > 40$ GeV), the S/B it is expected to be 2.4%. and the QCD contamination is small, decreasing from $\approx 10^{11}$ to $\approx 10^5$ after the $\not\!\!E_T$ cut. The next step requires a tight criteria for tau object selection, including the additional cuts:

- $N_\tau \geq$ 1: at least one tau (e/μ) with $p_T > 20$ GeV/c, $|\eta| < 2.4$, additional tau selection:
  - Jet Veto: Tracker and ECAL Isolation + Signal track size = one (**1-prong**) or three (**3-prong**);
  - Lepton Veto: EMF < 0.9, E/P > 0.5;
- Opposite Sign between lepton and tau leading track.
- Jet b-tagging;

Results are scaled to an integrated luminosity of 200 pb^{-1}: $N_{e\tau} \approx 50 \pm 2$ and $N_{\mu\tau} \approx 50 \pm 2$, of signal events are selected after the opposite sign (OS) cut for 1-prong tau decays (Tab. III). The uncertainties are statistical only, and the low value it is due to a rescaling of the integrated luminosity. The main sources of background at this stage of selection are from other-$t\bar{t}$ $\ell(q\bar{q})$ channel ($\approx 57 \pm 2$). The S/B is 0.71 and a better S/B ratio can be obtained after requiring b-tagging.

For the 3-prong selection (Tab. IV), $N_{e\tau} \approx 15 \pm 1$ and $N_{\mu\tau} \approx 15 \pm 1 \mu\tau$ event candidates are selected after the OS cut. The background of this channel it is from same order of magnitude as the **1-prong** selection.

Due to a flat distribution on the track multiplicity from QCD jets, the selection with **3-prong** taus has a lower signal significance and the S/B decreases from ≈ 0.8 with **1-prong** selection to ≈ 0.3 with **3-prong**.

The jet multiplicity distribution for signal and background events is shown in Fig. 8 (left). As expected, signal events of tau dilepton are predominant in the $N_{jet} \geq 2$ bin and the major background contamination arises from the W+jets events.

As the ttbar events exhibit a large hadronic activity, due to the large numbers of visible and invisible (neutrinos) objects involved in the decay chain, is is expected that the hadronic activity is higher for $t\bar{t}$ events than for the rest of background. The H_T distribution calculated before (after) the opposite sign (OS) cut is shown in Fig. 8 (right). It can be seen that

Table II: Number of expected events including trigger and W+jets-like selection for $\mathcal{L} = 200$ pb^{-1} ($\ell = e, \mu$). Uncertainties are statistical.

	channel	Init	Trigger	$N_{lep} \geq 1$	$N_{jet} \geq 2$	$\not\!\!E_T > 40$
signal $t\bar{t}$	$e\tau$	1547.6 ± 11.6	1306.4 ± 10.7	912.3 ± 8.9	728.1 ± 8.0	575.3 ± 7.1
	$\mu\tau$	1553.1 ± 11.7	1321.1 ± 10.7	927.8 ± 9.0	754.6 ± 8.1	592.0 ± 7.2
other $t\bar{t}$	$\ell(q\bar{q})$	28844.7 ± 50.2	24712.8 ± 46.5	16707.2 ± 38.2	15895.2 ± 37.3	11201.0 ± 31.3
	$\ell\ell$	5617.4 ± 22.2	5325.0 ± 21.6	4656.9 ± 20.2	3345.7 ± 17.1	2670.2 ± 15.3
	$\tau(q\bar{q})$	7951.3 ± 26.4	4466.8 ± 19.8	58.3 ± 2.3	54.3 ± 2.2	40.9 ± 1.9
	$\tau\tau$	441.9 ± 6.2	233.5 ± 4.5	5.3 ± 0.7	3.5 ± 0.6	2.9 ± 0.5
	full $-$ had	36844.1 ± 56.8	21640.4 ± 43.5	105.1 ± 3.0	102.7 ± 3.0	45.0 ± 2.0
other bkg	$W + jets$	7120000.0 ± 2280.7	2826860.3 ± 1437.1	2078525.7 ± 1232.3	53358.0 ± 197.4	28662.2 ± 144.7
	$Z(\ell\ell) + jets$	488006.6 ± 520.1	351376.4 ± 441.3	300342.6 ± 408.0	10340.8 ± 75.7	1978.9 ± 33.1
	$Z(\tau\tau) + jets$	211993.4 ± 342.8	54396.8 ± 173.6	17046.3 ± 97.2	1362.5 ± 27.5	528.8 ± 17.1
	Single Top	32800.0 ± 133.3	21705.9 ± 108.6	13082.5 ± 86.5	6267.4 ± 57.3	4064.0 ± 45.9
	QCD	$(3.1 \pm 0.0) \times 10^{11}$	$(2.5 \pm 0.0) \times 10^{9}$	$(9.9 \pm 0.0) \times 10^{9}$	$(1.0 \pm 0.1) \times 10^{9}$	$(1.8 \pm 0.5) \times 10^{5}$
	S/B	0.000	0.001	0.001	0.016	0.024
	$S/\sqrt{B}$	1.101	1.444	1.180	4.922	5.263

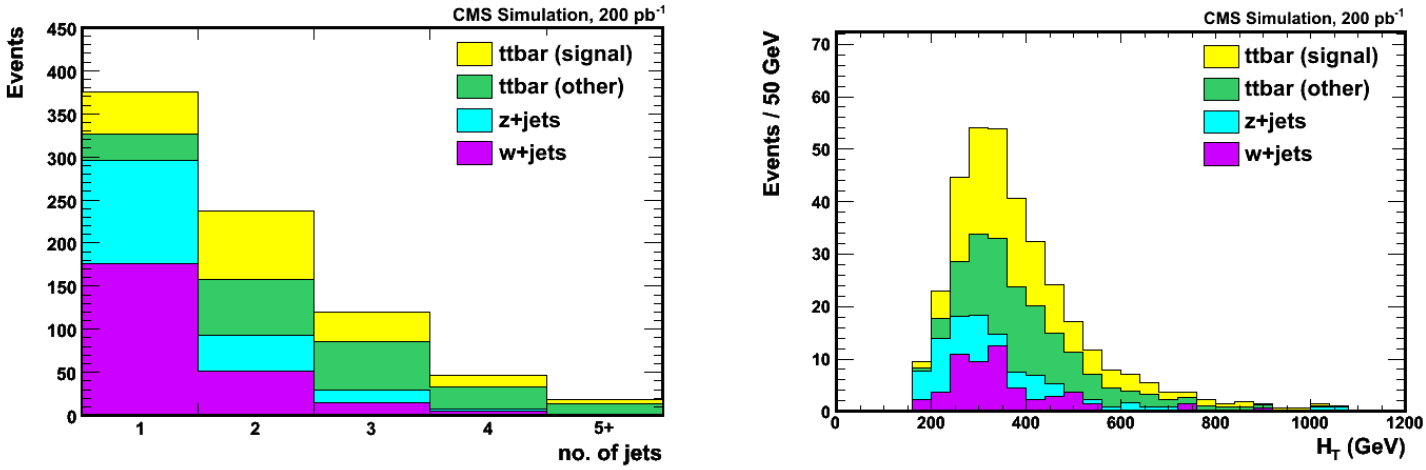

Figure 8: Jet multiplicity (left) and H_T (right) distributions for signal and background events for $\mathcal{L} = 200$ pb^{-1} after the OS cut.

the signal (yellow) it s not affected by this cut, while all the background (green, cyan, and magenta) decreases with the application of the OS cut.

6. BACKGROUNDS

Processes with at least one high-p_T lepton or jet, either mis-reconstructed or mis-labeled, may represent a background to the analysis. Most relevant backgrounds have been considered, and methods to estimate the fake contamination from data were exploited. A method that convolutes the τ-fakerate with W+jets-like $p_T \times \eta$ distribution, will be used to estimate the contamination from data.

A large background in the tau dilepton analysis comes from W+ ≥ 3 jets events where one jet is misidentified (τ-fake) as a tau. The background can come essentially from the following sources:

a) $t\bar{t}$ events, where the W boson and the jets are (mainly) from top decays;

b) W-boson production in association with QCD jets;

c) Z-boson production, particularly the case $Z \rightarrow (\tau\tau) \rightarrow \tau(\text{lep})\tau(\text{had})$ (irreducible background);

d) Single Top production in association with QCD jets;

In order to estimate the contribution of this background directly from data, a two-step process is used. First, the probability that a jet "fakes" a hadronically decaying tau lepton is evaluated from all jets in a jet-dominated sample (i.e. multi-jet and photon+jet), and it is parametrized as a function of jet p_T.

$$\text{fakerate} : \mathcal{P}(p_T, \eta)_{\tau|\text{jet}} = \frac{N_\tau(p_T, \eta)}{N\text{jet}(p_T, \eta)} \tag{7}$$

$$\begin{aligned} N_{W+\tau} &= \mathcal{P}(p_T, \eta)_{\tau|\text{jet}} \otimes N_{W+\text{jets}} \\ &= \int_{p_T^{min}}^{\infty} N_{W+\text{jets}} \times \frac{d\mathcal{P}(p_T, \eta)_{\tau|\text{jet}}}{dp_T} dp_T \end{aligned} \tag{8}$$

Table III: Number of expected events for $\mathcal{L} = 200$ pb^{-1} ($\ell = e, \mu$). Only 1-prong tau-tagged decays are considered. Uncertainties are statistical only.

	channel	Trigger+W-like	$N_{tau} \geq 1$	O.S.	$N_{btag} \geq 1$	$N_{btag} \geq 2$
signal $t\bar{t}$	$e\tau$	575.3 ± 7.1	50.4 ± 2.1	49.3 ± 2.1	43.4 ± 1.9	21.7 ± 1.4
	$\mu\tau$	592.0 ± 7.2	50.8 ± 2.1	49.8 ± 2.1	43.6 ± 2.0	21.9 ± 1.4
other $t\bar{t}$	$\ell(q\bar{q})$	11201.0 ± 31.3	72.2 ± 2.5	56.1 ± 2.2	46.8 ± 2.0	19.3 ± 1.3
	$\ell\ell$	2670.2 ± 15.3	12.0 ± 1.0	10.1 ± 0.9	8.7 ± 0.9	4.2 ± 0.6
	$\tau(q\bar{q})$	40.9 ± 1.9	1.8 ± 0.4	0.9 ± 0.3	0.6 ± 0.2	0.1 ± 0.1
	$\tau\tau$	2.9 ± 0.5	0.4 ± 0.2	0.3 ± 0.2	0.3 ± 0.2	0.3 ± 0.2
	full $-$ had	45.0 ± 2.0	0.3 ± 0.2	0.2 ± 0.1	0.1 ± 0.1	0.0 ± 0.0
other bkg	W + jets	28662.2 ± 144.7	35.8 ± 5.1	27.8 ± 4.5	5.1 ± 1.9	0.7 ± 0.7
	$Z(\ell\ell)$ + jets	1978.9 ± 33.1	16.1 ± 3.0	12.7 ± 2.7	1.1 ± 0.8	0.0 ± 0.0
	$Z(\tau\tau)$ + jets	528.8 ± 17.1	19.4 ± 3.3	18.8 ± 3.2	5.0 ± 1.7	1.7 ± 1.0
	Single Top	4064.0 ± 45.9	14.3 ± 2.1	11.5 ± 1.8	9.8 ± 1.8	2.9 ± 1.0
	QCD	180595.9 ± 45213.3	2.4 ± 0.7	1.0 ± 0.4	0.6 ± 0.3	0.2 ± 0.2
	S/B	0.005	0.580	0.711	1.115	1.482
	$S/\sqrt{B}$	2.435	7.660	8.394	9.849	8.035

Table IV: Number of expected events for $\mathcal{L} = 200$ pb^{-1} ($\ell = e, \mu$). Only 3-prong tau-tagged decays are considered. Uncertainties are statistical only.

	channel	Trigger+W-like	$N_{tau} \geq 1$	O.S.	$N_{btag} \geq 1$	$N_{btag} \geq 2$
signal $t\bar{t}$	$e\tau$	575.3 ± 7.1	15.9 ± 1.2	15.0 ± 1.1	13.7 ± 1.1	6.6 ± 0.8
	$\mu\tau$	592.0 ± 7.2	15.0 ± 1.1	14.6 ± 1.1	12.8 ± 1.1	6.9 ± 0.8
other $t\bar{t}$	$\ell(q\bar{q})$	11201.0 ± 31.3	66.9 ± 2.4	46.5 ± 2.0	38.1 ± 1.8	15.2 ± 1.2
	$\ell\ell$	2670.2 ± 15.3	3.6 ± 0.6	1.8 ± 0.4	1.2 ± 0.3	0.3 ± 0.2
	$\tau(q\bar{q})$	40.9 ± 1.9	0.6 ± 0.2	0.3 ± 0.2	0.3 ± 0.2	0.1 ± 0.1
	$\tau\tau$	2.9 ± 0.5	0.2 ± 0.1	0.1 ± 0.1	0.1 ± 0.1	0.1 ± 0.1
	full $-$ had	45.0 ± 2.0	0.7 ± 0.2	0.3 ± 0.2	0.3 ± 0.2	0.1 ± 0.1
other bkg	W + jets	28662.2 ± 144.7	36.5 ± 5.2	27.8 ± 4.5	3.7 ± 1.6	0.0 ± 0.0
	$Z(\ell\ell)$ + jets	1978.9 ± 33.1	2.2 ± 1.1	1.1 ± 0.8	0.6 ± 0.6	0.0 ± 0.0
	$Z(\tau\tau)$ + jets	528.8 ± 17.1	3.3 ± 1.4	2.8 ± 1.2	1.1 ± 0.8	0.0 ± 0.0
	Single Top	4064.0 ± 45.9	10.7 ± 2.1	7.8 ± 1.7	5.2 ± 1.4	2.5 ± 1.2
	QCD	180595.9 ± 45213.3	16.6 ± 7.1	11.5 ± 6.2	3.8 ± 3.6	0.0 ± 0.0
	S/B	0.005	0.219	0.295	0.489	0.737
	$S/\sqrt{B}$	2.435	2.604	2.956	3.599	3.150

The fake rate is calculated from the ratio of the p_T distribution of the jets which have satisfied the tau-tagging algorithm divided by the inclusive jet p_T distribution. This ratio gives the probability that each jet fakes a hadronically decaying tau lepton. The fake rate for all jets is shown in Fig. 9 after **isolation**, **1-prong** and **1- or 3-prong** selection cuts.

The fake rate of isolated tracks is calculated including all tau identification requirements. The isolation requirement in a cone (between R=0.07 and R=0.5) (Tracker + ECAL), reduces the fake probability by a factor of ~ 10. In order to evaluate the fake probability, the inclusive multi-jet sample with "all jets" has been used, as well as sub-samples including "leading jets", "next-to-leading jets", or "back-to-back jets" ($\Delta\phi^{\text{jet}-\text{jet}} > 2.4$) jets. The *all jets* category definition for fake probability is shown in Fig. 9.

The number of fake events (Eq. 8) is obtained by applying the fake probability (Eq. 7) to the p_T (and η) spectrum of all jets in the events passing the W+ ≥ 3 jet selection is shown in Fig. 10 (light red). Events are selected with the presence of at least one lepton (electron or muon, $p_T > 20$ GeV/c and $|\eta| < 2.4$), $\not{E}_T > 40$ GeV, $N^{30}_{\text{jet}} \geq 2$ (i.e. at least two jets with $p_T > 30$ GeV/c and $|\eta| < 2.4$), $N^{10}_{\text{jet}} \geq 1$ (i.e. at least one jet with $p_T > 10$ GeV/c and $|\eta| < 2.4$). The lower threshold for one jet is due to the tau. At least two jets which are not associated to the tau must be selected. Therefore, the fake probability is applied to all jets when $N_{\text{jet}}(p_T > 30 \text{ GeV/c}) > 2$, or only to the "tau" jet when $N_{\text{jet}}(p_T > 30 \text{ GeV/c}) = 2$.

The results for the total number of fakes were obtained with "standard" method before the OS cut is applied and are shown in Tab. V. Results are less than 10% from MC expectations.

In order to assign a charge to the leading track of the *tau*-like object, "taggable" jets can be used in the denominator, instead of using all jets. A "taggable" jet is selected to satisfy loose requirements ($E_T > 10$ GeV, with a leading track $p_T > 20$ GeV/c within $\Delta R < 0.1$ from the jet axis).

A W+ ≥ 3 "taggable" jet events distribution (Fig. 10 (light

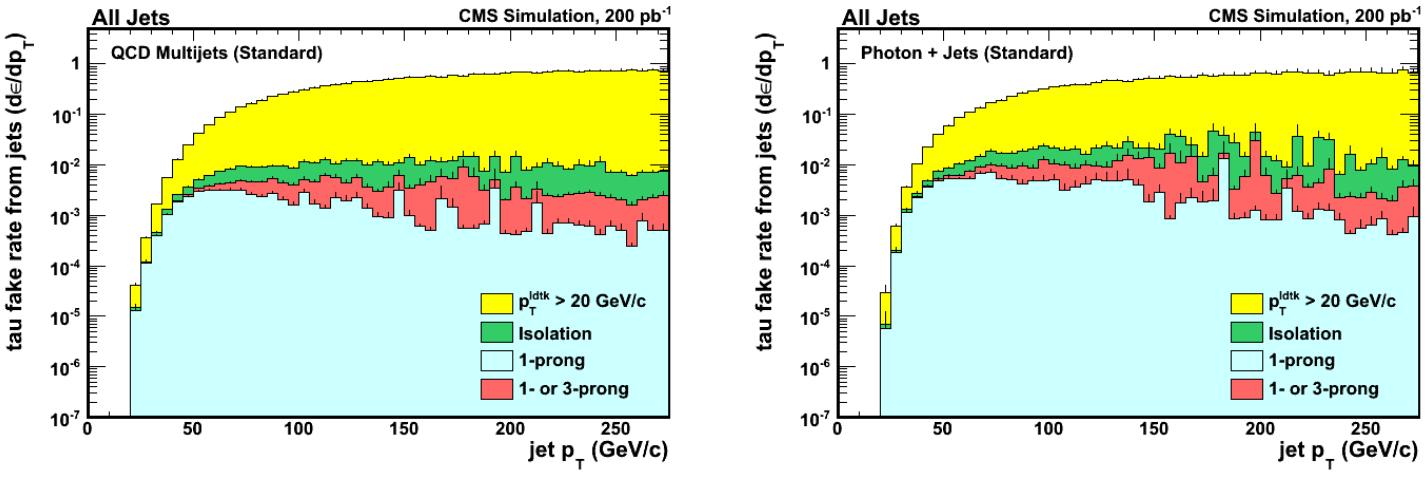

Figure 9: Left: Fake rate as function of jet transverse momentum for "all jets" in a multi-jet QCD (left) and photon+jets (right) samples after sequential selection cuts.

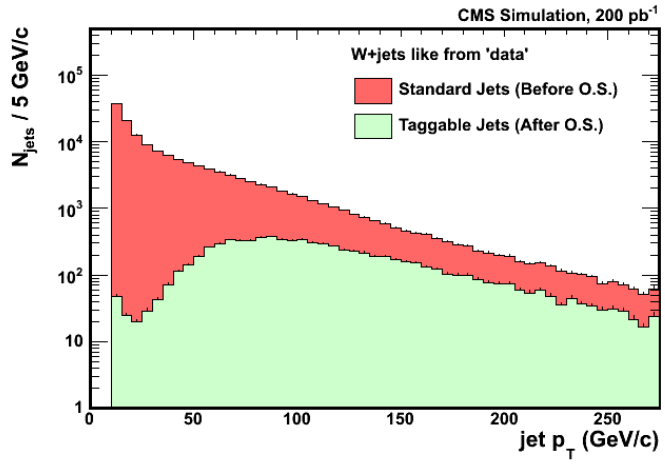

Figure 10: p_T (left) and η (right) distributions of "standard" and "taggable" jets in $W+ \geq 3$ jets events, before and after the OS cut.

Table V: "Standard" method: Expected number of τ-fake events (from data and from event selection) in $\mathcal{L} = 200$ pb^{-1} of data. Uncertainties are statistical only. The OS cut **is not** applied.

Method			τ-fakes from "data"	expected
1-prong	multi-jet QCD	"all" jets	135.0 ± 11.6	138.6 ± 6.5
		leading jet	153.3 ± 12.4	
		next-to-leading jet	77.4 ± 8.8	
		back-to-back jet	128.7 ± 11.3	
	photon+jets	"all" jets	274.6 ± 16.6	
		leading jet	286.8 ± 16.9	
		next-to-leading jet	171.7 ± 13.1	
		back-to-back jet	229.1 ± 15.1	
1- or 3-prong	multi-jet QCD	"all" jets	220.1 ± 14.8	249.3 ± 8.8
		leading jet	248.5 ± 15.7	
		next-to-leading jet	134.2 ± 11.6	
		back-to-back jet	210.4 ± 14.5	
	photon+jets	"all" jets	456.3 ± 21.3	
		leading jet	477.2 ± 21.8	
		next-to-leading jet	263.2 ± 16.2	
		back-to-back jet	342.4 ± 18.5	

green) is obtained. The number of τ-fakes estimated by the convolution of the fake rate with the p_T (η) distribution.

Results obtained after OS cut is applied are shown in Tab. VI. After calculating the average from multi-jet QCD ("all jets"), results are about $\sim 10\%$ (after OS cut) from MC expectations.

Table VI: "Taggable" method: Expected number of τ-fake events (from data and from event selection) in $\mathcal{L} = 200$ pb^{-1} of data. Uncertainties are statistical only. The OS cut **is** applied.

Method			τ-fakes from "data"	expected
1-prong	multi-jet QCD	"all" jets	108.5 ± 10.4	108.0 ± 5.8
		leading jet	111.7 ± 10.6	
		next-to-leading jet	65.1 ± 8.1	
		back-to-back jet	72.9 ± 8.5	
	photon+jets	"all" jets	146.6 ± 12.1	
		leading jet	147.9 ± 12.1	
		next-to-leading jet	86.9 ± 9.3	
		back-to-back jet	88.1 ± 9.4	
1- or 3-prong	multi-jet QCD	"all" jets	161.8 ± 12.7	186.1 ± 7.6
		leading jet	167.6 ± 12.9	
		next-to-leading jet	102.7 ± 10.1	
		back-to-back jet	121.0 ± 11.0	
	photon+jets	"all" jets	239.3 ± 15.5	
		leading jet	241.9 ± 15.5	
		next-to-leading jet	143.5 ± 12.0	
		back-to-back jet	121.9 ± 11.0	

7. CROSS SECTION

The $t\bar{t}$ cross section $\sigma_{t\bar{t}}$ with tau dilepton channel is performed after event yield and and of fake contribution form jets on the W+jets-like distribution estimation. Acceptance and systematic uncertainties, are estimated from Monte Carlo.

The numeric values of the acceptance of tau dilepton channel are calculated after each cut is applied. The total acceptance, A_{tot}, is presented in Eq. 9.

$$A_{tot} = A_{geom \cdot p_T} \times \epsilon_{trigger} \times \epsilon^{e,\mu}_{ID} \times \epsilon^{\tau}_{ID} \times \epsilon_{\not{E}_T} \times \epsilon_{OS} \times \epsilon_{b-tag} \quad (9)$$

The acceptances estimated from MC after OS cut, with respect to the generated channels are:

$$A_{tot} = [0.120 \pm 0.003(stat)]\% \quad \text{for } \mathbf{1-prong} \text{ tau decays}$$
$$A_{tot} = [0.036 \pm 0.002(stat)]\% \quad \text{for } \mathbf{3-prong} \text{ tau decays}$$

The main source of systematic uncertainties in the cross section measurement, is due to tau identification. With the calculation of cross sections ratio, $\mathcal{R} = \sigma^{\ell\tau}_{t\bar{t}}/\sigma^{e\mu}_{t\bar{t}}$, most of the systematic uncertainties will cancel out.

Systematic uncertainties due to tau identification are evaluated by varying the tau algorithm parameters by 10% around the default values. A smaller variation (2%) [10] is used as the uncertainty of the track p_T. Results are obtained from a

sample of $Z \to \tau\tau$ events and are listed in Tab. VII. For taus, uncertainties are accounted with $\eta - \phi$ direction deviations of the reconstructed track(s), as well as the deviations rising from the electron/muon veto cuts.

Additional systematic uncertainties, intrinsic to the method used for number of fakes estimation from "data", are evaluated by the calculation the maximum deviation of data-driven results to what is expected from Monte Carlo. This deviation, majored by 10%, will be used on fake estimation, propagated to the cross section measurement with the systematic from tau ID added in quadrature.

Table VII: Systematic uncertainties due to tau identification. Variations on different tau identification parameters were performed and the different sources were summed in quadrature.

Parameter (default ± variation)	$-\Delta$	$+\Delta$
$R_{sig}(0.1 \pm 10\%)$	+2.0%	-2.5%
$R_{iso}(0.5 \pm 10\%)$	-3.0%	+4.2%
$p_T^{leadTk}(20$ [GeV/c] $\pm 2\%)$	-2.6%	+2.5%
$p_T^{min}(1$ [GeV/c] $\pm 10\%)$	+2.7%	-2.7%
$EMF(< 0.9 \pm 10\%)$	+7.1%	-7.3%
$E/p^{leadTk}(> 0.5 \pm 10\%)$	-1.5%	+1.0%
Total	-8.9%	+10.4%

Table VIII: Estimated $t\bar{t}$ tau dilepton cross section for 1-prong or 1 and 3-prong tau decays.

	1-prong		1 and 3-prong	
	before OS	after OS	before OS	after OS
$N_{observed}$	259.2 ± 7.9	226.0 ± 7.2	404.2 ± 10.1	336.3 ± 9.0
N_{fakes}	$135.0^{\pm 11.6(sta)}_{\pm 27.0(sys)}$	$108.5^{\pm 10.4(sta)}_{\pm 21.7(sys)}$	$220.1^{\pm 14.8(sta)}_{\pm 44.0(sys)}$	$161.8^{\pm 12.7(sta)}_{\pm 32.4(sys)}$
$N_{Z\to\tau\tau}$ (MC)	19.4 ± 3.3	18.8 ± 3.2	22.7 ± 3.5	21.6 ± 3.5
N_{signal} (MC)	101.2 ± 3.0	99.1 ± 2.9	132.2 ± 3.4	128.7 ± 3.4
N_{signal} (data)	104.8 ± 10.2	98.7 ± 9.9	161.4 ± 12.7	152.9 ± 12.4
A_{tot} (%)	0.122 ± 0.004	0.120 ± 0.004	0.160 ± 0.004	0.155 ± 0.004
$\sigma_{t\bar{t}}$(data)(pb)	$428.7^{\pm 83.1(sta)}_{\pm 85.7(sys)}$	$412.2^{\pm 77.4(sta)}_{\pm 82.4(sys)}$	$505.5^{\pm 80.3(sta)}_{\pm 101.1(sys)}$	$491.9^{\pm 72.7(sta)}_{\pm 98.4(sys)}$
$\sigma_{t\bar{t}}$(MC)(pb)	414.0		414.0	

The $t\bar{t}$ production cross section $\sigma_{t\bar{t}}$ is estimated with Eq. 10, where $N_{observed}$ is the number of observed candidate events, N_{fakes} is the estimate of the background, $\mathcal{L}$ is the integrated luminosity, and A_{tot} is the total acceptance for tau dilepton, before and after OS cut.

$$\sigma_{t\bar{t}} = \frac{N_{observed} - N_{fakes}}{\mathcal{L} \cdot A_{tot}} \quad (10)$$

The cross section is estimated from signal events ($N_{signal} = N_{observed} - N_{fakes} - N_{Z\to\tau\tau}$) and for events passing the selection cuts. The $N_{Z\to\tau\tau}$ contribution, is considered irreducible background and it is estimated from Monte Carlo simulation with $Z \to \tau\tau$ events. The cross section results, together with number of signal and background events, are listed in Tab. VIII.

The estimated cross section with **1-prong** taus selection is, $\sigma_{t\bar{t}} = 428.7^{\pm 83.1(sta)}_{\pm 85.7(sys)}$ pb before the OS and $\sigma_{t\bar{t}} = 412.2^{\pm 77.4(sta)}_{\pm 82.4(sys)}$ pb after the OS cut.

8. CONCLUSIONS

A description towards the measurement of the $t\bar{t}$ cross section in tau dilepton channel with CMS detector was presented.

The object reconstruction was described, with particular interest in the taus. The expected yields after a full selection were obtained, and the statistical method, based on a fake probability to estimate the background contamination was described.

After a description towards the measurement of the $t\bar{t}$cross section with the first $\mathcal{L} = 200$ pb^{-1} LHC collisions at $\sqrt{s} = 10$ TeV, collected by the CMS detector with the dilepton channel with taus, approximately 130 $e\tau/\mu\tau$ $t\bar{t}$ dilepton events (**1- or 3-prong**) are expected to be found with the first $\mathcal{L} = 200$ pb^{-1} of collected data after OS selection. A signal-to-background ratio of S/B ≈ 0.72 (S/B ≈ 0.28) is found after full event selection for **1-prong** (**3-prong**) tau decays after opposite sign between lepton and the hadronically decaying tau. The observed is $\sigma_{t\bar{t}} = 412.2^{\pm 77.4(sta)}_{\pm 82.4(sys)}$ pb after the OS.

[1] C. Amsler et al. Review of particle physics. *Phys. Lett.*, B667:1, 2008.

[2] F. Abe et al. Observation of Top Quark Production in $p\bar{p}$ Collisions with the Collider Detector at Fermilab. *Phys. Rev. Lett.*, 74(14):2626–2631, Apr 1995.

[3] S. Abachi et al. Observation of the Top Quark. *Phys. Rev. Lett.*, 74(14):2632–2637, Apr 1995.

[4] Roberto Bonciani, Stefano Catani, Michelangelo L. Mangano, and Paolo Nason. NLL resummation of the heavy-quark hadroproduction cross- section. *Nucl. Phys.*, B529:424–450, 1998.

[5] M. Cacciari, S. Frixione, M. L. Mangano, P. Nason, and G. Ridolfi. Updated predictions for the total production cross sections of top and of heavier quark pairs at the Tevatron and at the LHC. *JHEP*, 09:127, 2008.

[6] A. Abulencia et al. A search for $t \to \tau\nu q$ in $t\bar{t}$ production. *Phys. Lett.*, B639:172, 2006.

[7] F. Abe et al. The $\mu\tau$ and $e\tau$ decays of top quark pairs produced in $p\bar{p}$ collisions at $\sqrt{s} = 1.8$ TeV. *Phys. Rev. Lett.*, 79:3585–3590, 1997.

[8] CMS Collaboration. CMSSW CVS and TWiki page:. http://cmssw.cvs.cern.ch/ https://twiki.cern.ch/twiki/bin/view/CMS/WorkBook.

[9] CMS Collaboration. Physics Analysis Toolkit TWiki page:. https://twiki.cern.ch/twiki/bin/view/CMS/SWGuidePAT .

[10] CMS Collaboration. *CMS Physics Technical Design Report, Volume. I: Detector Performance and Software*, June 2006. CERN/LHC 2006-021.

[11] J. Branson, M. Gallinaro, P. Ribeiro, R. Salerno, and M. Sani. A cut based method for electron identification in cms. *CMS Analysis Note*, 2008/082, 2008.

[12] CMS Collaboration. *CMS Physics Technical Design Report, Volume. II: Physics*, June 2006. CERN/LHC 2006-021.

[13] Gavin Salam and Gregory Soyez. The Seedless Infrared Safe Cone Jets. http://projects.hepforge.org/siscone/.

[14] Robert Harris et al. Plans for Jet Energy Corrections at CMS. *CMS Analysis Note*, CMS AN-2007/055, 2007.

[15] A. Rizzi, F. Palla, and G. Segneri. Track impact parameter based b-tagging with cms. *CMS Note*, 2006/019, 2006.

[16] CMS Collaboration. Probing the Heavy Flavor Content of the $t\bar{t}$ dilepton channel in proton proton collisions at $\sqrt{s} = 10\,TeV$. *CMS Analysis Note*, CMS AN-2008/112, 2009.

[17] CMS Collaboration. "$\not{E}_T$ performance in cms". *CMS PAS*, JME_07_001, 2007.

[18] S. Gennai et al. Tau jet reconstruction and tagging at high level trigger and off-line. *CMS Analysis Note*, 2006/028, 2006.